Catalysis Today 279 (2017) 209–216

Contents lists available at ScienceDirect

Catalysis Today

journal homepage: www.elsevier.com/locate/cattod

Mixed oxides tuned with alkaline metals to improve glycerolysis for sustainable biodiesel production

Nancy F. Balsamo[a], Karim Sapag[b], Marcos I. Oliva[c], Gina A. Pecchi[d], Griselda A. Eimer[a], Mónica E. Crivello[a,*]

[a] Centro de Investigación y Tecnología Química-Universidad Tecnológica Nacional-CONICET-Facultad Regional Córdoba, Córdoba, Argentina
[b] Instituto de Física Aplicada – Universidad Nacional de San Luis, San Luis, Argentina
[c] Instituto Enrique Gabiola-Facultad de Matemática Astronomía y Física-Universidad Nacional de Córdoba, Córdoba, Argentina
[d] Departamento de Físico-Química, Facultad de Ciencias Químicas, Universidad de Concepción, Concepción, Chile

ARTICLE INFO

Article history:
Received 1 December 2015
Received in revised form 19 May 2016
Accepted 1 June 2016
Available online 18 June 2016

Keywords:
Mixed metal oxides
Alkaline metals
Layered double hydroxides
Glycerol
Monoglycerides

ABSTRACT

In this study, monoglycerides were produced as glycerol value-added products via transesterification reaction of methyl stearate. This green and selective process involved catalysis from hydrotalcite-like compounds with different metals incorporated (Li, K or Cs) to improve their basic properties. Layered double hydroxides were obtained by two different methods and activated by calcination. All samples were examined by X-ray diffraction, specific surface area determined by the BET method, temperature-programmed desorption of CO_2 and infrared absorption spectroscopy with Fourier transform for basic sites measurement. Metal content was determined by inductively coupled plasma optical emission spectroscopy, energy dispersive X-ray spectroscopy and X-ray photoelectron spectroscopy. The hydrotalcite-like compounds modified with monovalent metal ions (Li, K or Cs) with the lamellar structure were synthesized. The metal percentage incorporated was higher for materials modified with Li than for those modified with K and Cs. This fact can be attributed to the lower size of their ionic radii. All mixed oxides presented basic properties. The products were analyzed by gas chromatography. The correlation between the basic properties of the solid catalysts and the activity in the transesterification reaction was investigated. The highest activity was found for the catalyst with Li incorporated by the co-precipitation method with yield values around 78% for monoglycerides. Which also showed the greatest Lewis medium basic sites density, a 31% more than the rest of the materials.

1. Introduction

A growing interest in the preparation of biofuels from biomass is emerging due to the increased concern about environmental issue [1,2]. In this context, biodiesel has gained considerable attention as a nontoxic, biodegradable and renewable alternative to petroleum-derived fuels. Biodiesel is usually manufactured by transesterification of plant and animal oils with methanol or ethanol, with glycerol as a coproduct [2]. The increase in biodiesel production is generating high amounts of glycerol. Consequently, the price of glycerol has dropped dramatically [3]. Thus, it is desirable to convert low-cost glycerol into value-added chemicals or materials. In addition, glycerol is an environmentally friendly compound containing a highly multifunctional structure, making it a versatile building block for the synthesis of a broad family of valuable derivatives by several catalytic processes involving oxidation [4,5], hydrogenolysis [6–8], dehydration [9], etherification [10], etc. The cost of biodiesel production is still an important aspect. In a first stage, glycerol can be used to reduce the acidity content of the feedstock by the esterification reaction, as Felizardo reported.

One of the promising routes to glycerol valuation is its catalytic esterification to produce monoglycerides, which are important fine chemicals for food, detergent, plasticizer, pharmaceutical and cosmetic formulations [11].

Monoglycerides, the glycerol monoesters, can be obtained by the transesterification (glycerolysis) of fatty methyl esters with glycerol or by the direct esterification of glycerol with fatty acids. However, the three hydroxyl groups in glycerol are not very different in reactivity, thus the product of the direct esterification or transesterification of glycerol with acid and/or base catalysts is a

* Corresponding author.
E-mail addresses: mcrivello@frc.utn.edu.ar, mcrivello@scdt.frc.utn.edu.ar, elsiecrivello@hotmail.com (M.E. Crivello).

http://dx.doi.org/10.1016/j.cattod.2016.06.005
0920-5861/

mixture of mono-, di-, and sometimes triglycerides depending on the catalyst performed, plus the glycerol that has not reacted.

Heterogeneous catalysis has gained importance in the field of basic catalysis, and different materials such as oxides [12–16], hydroxides [17] and organic modified mesoporous materials [18] have been studied. For this purpose, layered double hydroxides (LDH) have probably been the most studied materials as basic catalysts in the last few years, and there is a vast literature concerning catalysis with this kind of material [19]. Nowadays, hydrotalcite-like compounds have gained special relevance in the transesterification of oils for biodiesel synthesis [20].

LDH are bidimensional anionic clays with an alternating layered structure with positively charged brucite-type layers, where Mg^{2+} cations are substituted by Al^{3+} cations and the interlayers contain the charge balancing anions and water molecules. These compounds are represented by the formula $(M_{(1-x)}{}^{2+}M_x{}^{3+}(OH)_2)^{x+}(A_{x/n}{}^{n-}mH_2O)^{x-}$, where the divalent ion may be Mg^{2+} or monovalent ions such as Li^+, K^+, Cs^+, and the trivalent ion Al^{3+}, Fe^{3+} or Cr^{3+}. The compensating anion (A^{n-}) may be $CO_3{}^{2-}$, $NO_3{}^-$, Cl^-, $SO_4{}^{2-}$, and x can take values between 0.25 and 0.33.

Conventional hydrotalcites generally show low catalytic activity in their original form, but through controlled thermal decomposition, LDH are converted to mixed oxides with high specific surface areas and strong basic sites [21,22]. The basicity can be tuned, and other catalytic properties can be imparted through the incorporation of a range of catalytically active metals in the brucite lattice structure [23–25].

In this paper, the influence of alkaline metals on the structural and catalytic properties of the samples has been studied. These materials were used in the transesterification (glycerolysis) of methyl stearate with glycerol. The precursors and mixed oxides were characterized by different physicochemical methods, such as X-ray powdered diffraction (XRD), specific surface determined by the BET method. The chemical composition of mixed oxides was analyzed by inductively coupled plasma optical emission spectroscopy (ICP-OES), energy dispersive analysis (EDS) and X-ray photoelectron spectroscopy (XPS) for the lithium samples. The density and strength of basic sites of mixed oxides were determined by CO_2 probe molecule, which is one of the most widely used to characterize basic surfaces by infrared absorption spectroscopy with Fourier transform (FT-IR) [26] and temperature-programmed desorption (TPD) [27]. Moreover, the products of transesterification were analyzed by gas chromatography.

2. Material and methods

2.1. Synthesis

The preparative methods adopted in this study were direct co-precipitation and impregnation. In the direct co-precipitation method, the samples were prepared by the low supersaturation method at constant pH (10 ± 0.2), with M^{2+}/M^{3+} constant molar ratio of 3, according to the procedure reported by us elsewhere [22]. Two solutions were prepared. One of them contained $Mg(NO_3)_2{\cdot}6H_2O$, $Al(NO_3)_3{\cdot}9H_2O$ and the nitrate of the alkaline metal to incorporate them dissolved together in distilled water and the other, 0.085 M of Na_2CO_3 in distilled water. Both solutions were dropped simultaneously into 50 mL of distilled water at 60 mL h^{-1}. The pH was kept constant by adding a 2 M NaOH solution. The co-precipitation was carried out at room temperature, and the gel was continuously stirred magnetically. The mixture was kept under magnetic stirring for 4 h. The precipitate was aged in the mother liquor overnight at room temperature, and then the precipitate was separated and washed with distilled water, by centrifugation at 2800 rpm, until pH 7. The resulting material was dried overnight at 90 °C in the open air. Finally, the solids were calcined in open air at 450 °C for 9 h [22].

In the impregnation method, a salt aqueous solution of the metal ions was added to the Mg-Al mixed oxide obtained by co-precipitation. The theoretical metal loading was 10 wt%. The suspension was kept under stirring at room temperature for 20 min and then, it was dried in a vacuum rotary evaporator. The resulting solid was dried at 90 °C overnight, then it was calcined in air flow at 350 °C for 2 h and finally, at 500 °C for 8 h [23].

LDH samples and mixed metal oxide (MMO) samples were named by the symbol of the third metal incorporated followed by Mg-Al, and the symbol used as subindex corresponds to the synthesis method: co-precipitation (C) and impregnation (I). Thus, in the case of the sample with lithium incorporated: $(Li\text{-}Mg\text{-}Al)_C$, $(Li\text{-}Mg\text{-}Al)_I$.

2.2. Characterization

All samples were examined by XRD on a Philips PW 3838 diffractometer, using monochromatic Cu K radiation (λ= 1.54 Å) at a scan speed/rate of ¼° min-1 in a range between 10° and 80° and a step size of 0.02°.

The specific surface areas were measured using a Micromeritics ASAP 2000 instrument by single point at P/P0 = 0.3 through the BET method. The precursors were degassed at 200 °C and the calcined materials at 390 °C, both for 50 min.

The scanning electron microscopy (SEM) studies of the MMO were performed with a JEOL JSM-6380 LV, coupled with an energy dispersion analyzer (EDX) Oxford Instruments model 7582. The specimens were Au coated (sputtering) to make them conductive. The SEM acceleration voltage was 20 kV.

The X-ray photoelectron spectroscopy (XPS) measurements were carried out using a multitechnique system (SPECS) equipped with a dual Mg/Al X-ray source and a hemispherical PHOIBOS 150 analyzer operating in the fixed analyzer transmission (FAT) mode. The spectra were obtained with pass energy of 30 eV and a Mg anode operated at 100W. The working pressure in the analyzing chamber was less than 2.0×10^{-8} mbar. Samples were supported on double-sided Cu tape and previously evacuated for 12 h.

The MMO chemical composition was determined by inductively coupled plasma optical emission spectroscopy (ICP-OES). The equipment was a VISTA-MPX CCD Simultaneous ICP-OESVARIAN.

The catalyst basic properties were measured by temperature-programmed desorption (TPD) and Fourier transform infrared spectroscopy (FTIR) of CO_2. Typically, about 100 mg of the sample is placed in a quartz reactor and pretreated in argon at 100 °C for 60 min prior to the adsorption of CO_2 at the same temperature. After the adsorption of carbon dioxide (3 wt% CO^2 in He; 20 cm^3 min^{-1}) for 60 min, the catalyst was treated with a flow of helium (20 cm^3 min^{-1}) for 45 min at 100 °C in order to remove physically adsorbed CO_2. The CO_2-TPD desorption was measured by heating the sample from room temperature to 900 °C at a heating rate of 10 °C min^{-1}. The CO_2 uptake was determined by integrating the detected peaks using the software of the equipment previously calibrated with different amounts of Na_2CO_3. The CO_2 desorbed was analyzed and quantified by an on-line gas chromatograph (Shimadzu GC-14A) equipped with a TCD.

The structure of CO_2 chemisorbed on the sample was determined by infrared spectroscopy (IR). Data were obtained using a Shimadzu FTIR–8101 M spectrophotometer after CO2 adsorption at room temperature and sequential evacuation at 25, 100, 200, 300, and 400 °C. Spectra were taken at room temperature. An inverted T-shaped Pyrex cell containing the sample pellet was used. The two ends of the short arm of the T were fitted with CaF_2 windows. Finally, the difference spectrum for each sample was obtained by

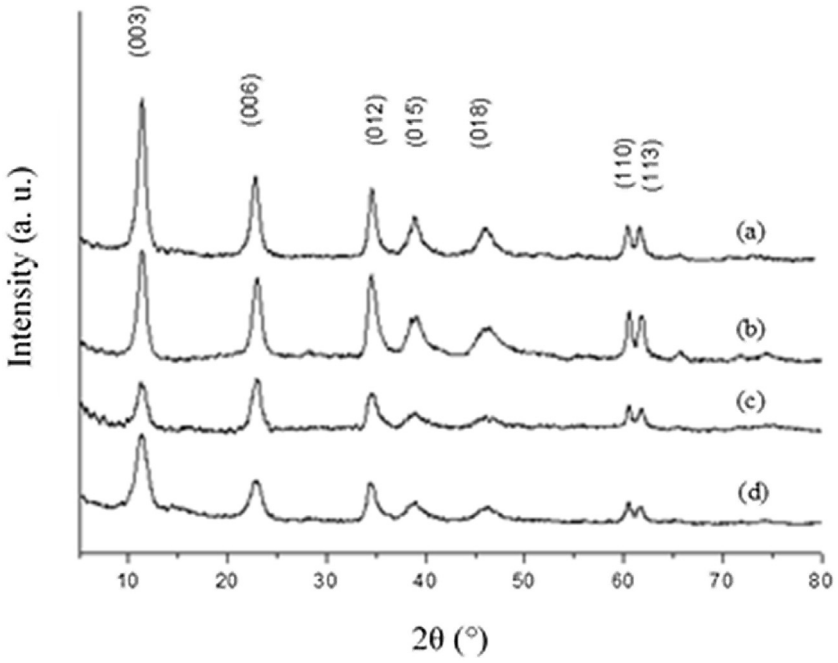

Fig. 1. XRD patterns of the LDH obtained by co-precipitation method. (a) $(Mg\text{-}Al)_C$, (b) $(Li\text{-}Mg\text{-}Al)_C$, (c) $(K\text{-}Mg\text{-}Al)_C$, (d) $(Cs\text{-}Mg\text{-}Al)_C$.

subtracting the background recorded previously. The absorbance scales were normalized to 50-mg pellets in a JASCO 5300 spectrometer equipped with a DTGS detector. The FT-IR spectra in the lattice vibration region were performed using the KBr 0.05% wafer technique.

2.3. Catalytic test

The transesterification reactions were performed in a glass batch reactor (20 mL) equipped with a condenser system to remove the methanol generated during the reaction.

The reactor was operated in a batch regime for the solid and liquid phases at atmospheric pressure under flowing N_2 (35 mL min^{-1}). A nitrogen purge was used to remove methanol from the reactor and to provide an inert atmosphere to avoid degradation of reactants and products. First, the reactants, glycerol (Cicarelli, 99%) and methyl stearate (Aldrich, >96%), were introduced and the reactor was flushed with nitrogen, and then, they were heated to the reaction temperature (220 °C) in a silicone bath and under stirring (500 rpm). After that, the catalyst as powder (4 wt%) form was added [28].

A glycerol/methyl stearate molar ratio of 6:1 was used. Although the stoichiometric molar ratio for the reaction is 1:1, an excess of glycerol was used to direct the reaction and increase methyl ester conversion. Reaction products were analyzed by gas chromatography (GC) after silylation to improve compound detectability. A proper and unique combination of silylating agents for the trimethylsilylation of the free hydroxyl groups of glycerol, mono- and diglycerides was used as well as the internal standard tricaprin. Silylating agents N,O-bis(trimethylsilyl)-acetamide (BSA, Fluka, >95%) and Trimethylchlorosilane (TMCS, Fluka, >98%) were used following the derivatization method described by Ferretti et al. [29]. Quantification was carried out using standards 1-steoryl-rac-glycerol (Sigma, >99% GC), Glyceryl 1,3-distearate (Sigma, >99%GC) and Glyceryl tristearate (Sigma, ≥99% GC). Silylated samples of products and reactants with a known amount of tricaprin (Glyceryl tridecanoate >99% GC Sigma) added as an internal standard were analyzed by gas chromatography using a Perkin Elmer gas chromatograph equipped with a capillary column (ZB-5HT Inferno™, 15 m length × 0.53 mm i.d.) and a flame ionization detector. Conversion and selectivity were expressed in moles%, and the yield was calculated as the product between them.

3. Results and discussion

3.1. Characterization of materials

3.1.1. XRD of precursors and oxides obtained by co-precipitation method

The precursor samples were analyzed by XRD to assess the presence of a crystalline structure depending on the method of synthesis employed. The peaks recorded are attributed to crystalline planes of a hydrotalcite structure. As is shown in Fig. 1, the XRD patterns of LDH synthesized by co-precipitation display the typical diffraction peaks at $2\theta \approx 11°$, 22°, and 35°, corresponding to the (0 0 3), (0 0 6) and (0 1 2) crystal planes in the layered structures with a rhombohedral symmetry (3R). The LDH diffraction patterns of all samples synthesized by co-precipitation have the typical structure of the hydrotalcite phase (PCPDFWIN 70-2151) regardless of the incorporated metal.

By comparing the XRD patterns, it can be seen that the sharpness of the peaks, directly related to crystallinity [30], decreases when the third metal is incorporated. This is more remarkable with the addition of K and Cs, which can be attributed to the increase in size of the ion radium of these cations [30].

Table 1 summarizes LDH cell parameters calculated from precursors by both methods. The parameter "*c*" indicates the basal spacing, and the parameter "*a*" is the cation-cation average distance of the laminar structure. These parameters were calculated using the reflections (003) and (110), and the equations $c = 3d_{003}$ and $a = 2d_{110}$. The analysis of the parameter "*a*" in LDH synthesized by co-precipitation shows no difference in its value, regardless of the metal ion used. In the case of the parameter "*c*", considering the width of the layer constant, it increased from 23.25 to 23.92 Å, showing that the interlayer distance (d_{003}) increases possibly due to the decrease in the electronegativity of the metal incorporated and the corresponding attraction between the layers.

Table 1
Cell parameters of LDH and specific surface area from LDH and MMO by both methods obtained.

Sample	a (Å)	c (Å)	d_{003}	Area ($m^2\ g^{-1}$)	
				LDH	OMM
$(Mg\text{-}Al)_C$	3.06	23.46	7.82	78	270
$(Li\text{-}Mg\text{-}Al)_C$	3.06	23.25	7.75	113	268
$(K\text{-}Mg\text{-}Al)_C$	3.06	23.55	7.85	138	282
$(Cs\text{-}Mg\text{-}Al)_C$	3.06	23.92	7.97	160	283
$(Mg\text{-}Al)_I$	3.04	23.70	7.90	3.2	318
$(Li\text{-}Mg\text{-}Al)_I$	3.07	19.22	6.41	1.7	142
$(K\text{-}Mg\text{-}Al)_I$	3.07	19.22	6.41	13	150
$(Cs\text{-}Mg\text{-}Al)_I$	3.08	18.94	6.31	39	225

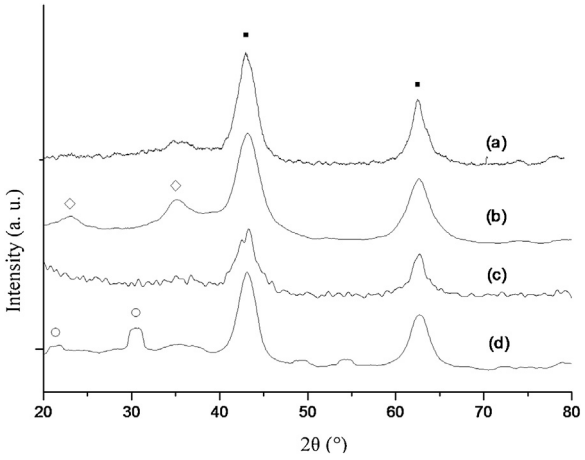

Fig. 2. XRD patterns of the OMM obtained by calcination from LDH synthesized by co-precipitation. (a) $(Mg\text{-}Al)_C$, (b) $(Li\text{-}Mg\text{-}Al)_C$, (c) $(K\text{-}Mg\text{-}Al)_C$, (d) $(Cs\text{-}Mg\text{-}Al)_C$. (■)MgO periclase, (◊) Li_2O, (◯) Cs_2O.

Calcined samples obtained by the co-precipitation method were analyzed by XRD to study the different oxide phases formed. Fig. 2 shows the X-ray diffraction patterns of the mixed metal oxides with the third metal incorporated, together with the diffraction pattern of the Mg-Al mixed oxide. After calcination at 450 °C, the reflections of basal planes (003) and (006) disappear. This is due to the rupture of the laminar structure and the release of H_2O in conjunction with the anion CO_3^{2-} as CO_2. All patterns showed the presence of MgO in periclase phase [31]. Furthermore, typical peaks of Li_2O and Cs_2O were observed. Species of K_2O were not detected. This could indicate that if potassium is incorporated in the structure, its oxide is dispersed in the material without forming large aggregates.

3.1.2. XRD of precursors and oxides obtained by impregnation method

X-ray diffraction patterns of the samples obtained by the impregnation method are shown in Fig. 3, where the LDH $(Mg\text{-}Al)_C$ and their oxide were included for comparing the patterns. The memory effect is the property of mixed oxides from hydrotalcite-like compounds calcined at temperatures no higher than 450 °C, which are capable of recovering their original structure [32–35]. This occurs when they are placed in contact with water, water vapor or another aqueous solution. The LDH $(Mg\text{-}Al)_I$ diffraction pattern shows wide and low peaks, indicating that the structure was partially regenerated. This behavior could be attributed to the short contact time between the Mg-Al oxide and distilled water [36]. The diffraction patterns of the rehydrated materials with the third metal incorporated showed partial recovery of the layer structure too. This could be due to the short contact time between the Mg-Al mixed oxide and the metal salt solution and because no washing process was performed to the samples [37]. Anyway, the purpose

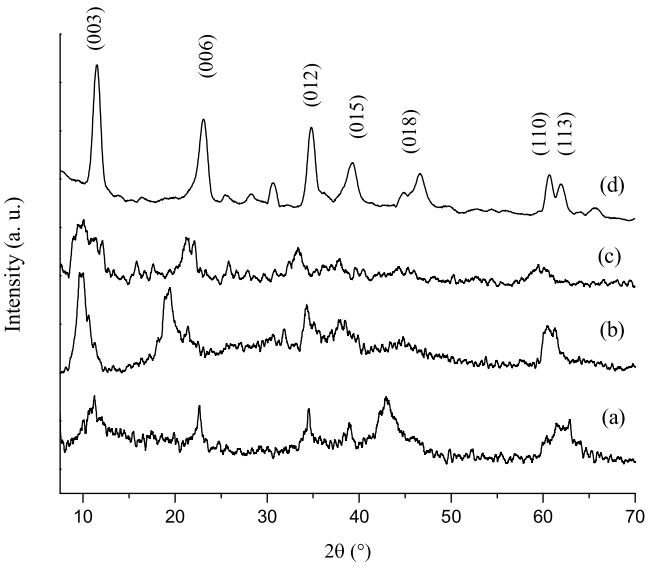

Fig. 3. XRD patterns of the LDH obtained by impregnation method. (a) $(Mg\text{-}Al)_I$, (b) $(Li\text{-}Mg\text{-}Al)_I$, (c) $(K\text{-}Mg\text{-}Al)_I$ y (d) $(Cs\text{-}Mg\text{-}Al)_I$.

of rehydration with the cationic solution is to incorporate the third metal by impregnation rather than to rebuild the layer structure. The parameters "*a*" and "*c*" in LDH synthesized by impregnation (Table 1) were modified when the third metal was incorporated. In the case of the parameter "*a*", there is a change in the values that could be attributed to increased planar defects produced during the recrystallization. Furthermore, the parameter "*c*" shows a decrease in the interlayer distance due to the clutter produced by different anions in the interlayer space.

Fig. 4 shows X-ray diffraction patterns of mixed oxides with an embedded third metal synthesized by the impregnation method. In all cases, the MgO periclase phase (PCPDFWIN 78-0430) was detected. In the diffraction patterns of Li modified samples, oxide crystalline phases were obtained, and Li_2O, Li_2CO_3 and the $LiAlO_2$ mixed oxide were detected. In the sample containing Cs, the formation of Cs_2O was not detected. Meanwhile, in the sample containing potassium, K_2O was detected. A comparison of the diffraction patterns shows that the sharpness of the peaks decreases as the metal ion size increases. By comparing the diffraction patterns of the mixed metal oxides obtained by both methods (Figs. 2 and 4), more crystalline phases were observed after rehydration (impregnation method). The several lithium phases detected could be attributed to the size of its ion radium, similar to the magnesium one.

3.1.3. Specific surface area

Table 1 lists the specific surface area values of the mixed oxides and their precursors obtained by the co-precipitation and impregnation methods. The oxide area was higher than the LDH one in all samples. This phenomenon is due to the destruction of the brucite-type layer together with the elimination of carbonate anions and water from the interlayer space. The carbonate anion is released as carbon dioxide, promoting the formation of small channels or pores in the solid, which increases the surface area [38]. Oxide and LDH specific surface areas increase when the metal ion radium increases.

3.1.4. Chemical composition

The chemical composition of mixed oxides obtained by both synthesis methods was analyzed by ICP, EDX and XPS techniques. Surface composition data are reported according to the possibility of the techniques to identify the third metal ion incorporated.

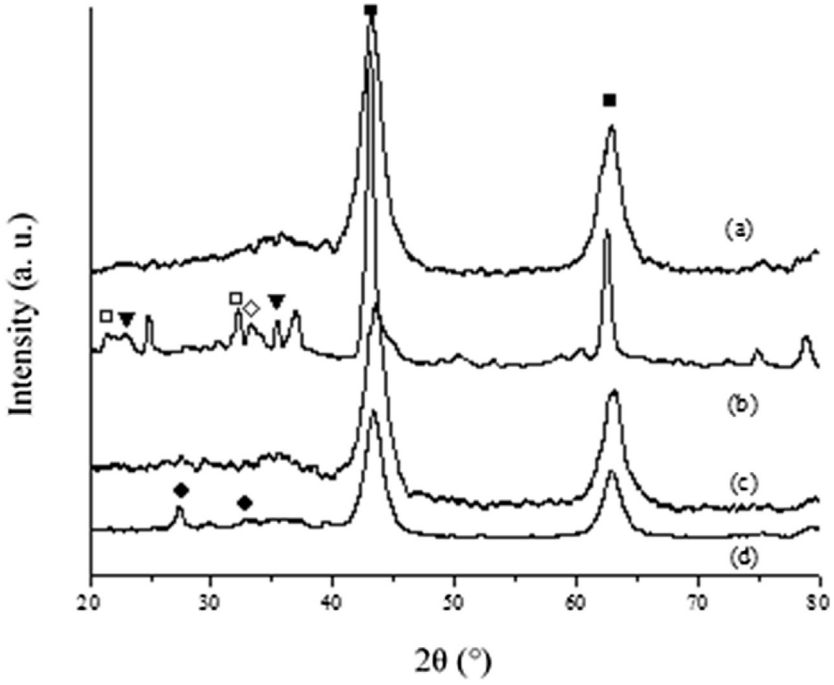

Fig. 4. XRD patterns of the OMM obtained by calcination from LDH synthesized by impregnation. (a) $(Mg\text{-}Al)_I$, (b) $(Li\text{-}Mg\text{-}Al)_I$, (c) $(Cs\text{-}Mg\text{-}Al)_I$, (d) $(K\text{-}Mg\text{-}Al)_I$, (■)MgO, (□)$Li_2CO_3$, (◊)$Li_2O$, (▼) $LiAlO_2$, (●) K_2O.

Table 2
Chemical composition of mixed oxides synthesized by both methods.

Sample	Molar ratio $(Mg^{2+}+M^+)/Al^{3+}$			% mol M^+		
	Synthesis	Bulk	Surface	Synthesis	Bulk	Surface
$(Mg\text{-}Al)_C$	3.00	2.56	–	–	–	–
$(Li\text{-}Mg\text{-}Al)_C$	3.00	2.55	3.96	15.00	13.00	34.49
$(K\text{-}Mg\text{-}Al)_C$	3.00	3.10	2.41	15.00	1.24	0.35
$(Cs\text{-}Mg\text{-}Al)_C$	3.00	2.98	2.00	15.00	1.38	2.76
$(Mg\text{-}Al)_I$	2.56	2.41	–	–	–	–
$(Li\text{-}Mg\text{-}Al)_I$	4.00	3.81	1.23	36.02	49.25	36.59
$(K\text{-}Mg\text{-}Al)_I$	2.82	3.71	1.10	9.09	7.50	4.32
$(Cs\text{-}Mg\text{-}Al)_I$	2.64	2.79	4.61	2.85	5.83	3.64

Thus, in the sample with K incorporated by co-precipitation, EDX was performed because it was undetectable by XPS [39].

Table 2 shows the chemical composition of MMO synthesized by both methods. For the materials synthesized by the co-precipitation method, the theoretical molar ratio, $(Mg^{2+}+M^+)/Al^{3+}$, was kept constant and equal to 3.

The theoretical molar ratio for the samples synthesized by the impregnation method was calculated from the Mg-Al oxide composition value experimentally obtained by ICP, and the theoretical number of moles of the third metal to incorporate was added. Table 2 also shows the molar% of the third metal incorporated (M^+ molar%), considering the $M2^+$ and M^+ metal ion amount of moles as total molar reference. ICP results revealed that the values found for the molar ratio of the Mg-Al oxides were close to the theoretical ones. In addition, the molar ratios in the MMO with the third metal incorporated by co-precipitation were similar to those of the synthesis. Meanwhile, Li percentage, determined by ICP for samples synthetized by co-precipitation, was essentially similar to that of the synthesis. However, through XPS, a high Li percentage was determined at surface level. In the case of K and Cs incorporated by co-precipitation, it was found that although the ionic molar ratio was keep close to that of the synthesis, the percentage of ions incorporated was close to 10% of the theoretical value for both metals by ICP. Meanwhile, in the MMO obtained by impregnation, it was observed that the ionic ratio in the samples with Li and Cs incorporated were closer to the theoretical one than those obtained for the sample with K incorporated. The surface molar ratio for the samples with the third metal incorporated by impregnation showed significantly lower values in the samples with Li and K incorporated. However, the microanalysis result for the Cs modified sample showed that the value of the ratio markedly increased [39].

Therefore, by comparing the composition results of the samples obtained by both synthesis methods, there was a higher proportion of third-level metal on the surface by the impregnation method.

3.1.5. Basic sites

The surface basicity of composite oxide catalysts was measured by CO_2-TPD, and the basic species could be assigned according to the temperature at which the peaks appeared. CO_2-TPD profiles for mixed oxide samples are shown in Fig. 5. The complex desorption profiles are clearly related to the presence of basic sites with different strengths. The basicity of an oxide surface is generally related to the electrodonating properties of the combined oxygen ions, so that when the partial negative charge on the combined oxygen ions is higher, the oxide is more basic.

As was reported by León [40], the formation of different species stems from the presence of sites with different basic strength in the CO_2 adsorption and desorption process: bicarbonates (OH^-, weak basic sites), bidentate carbonates (bridging, M^{m+}—O^{2-} pairs, medium-strength basic sites) or unidentates (O^{2-}, strong basic sites). Associating these types of species with the CO_2 desorption temperature reveals: (i) A low temperature peak, with a maximum of desorption between 100 and 210 °C, attributed to the interaction with sites having weak basic strength. (ii) A desorption peak with a maximum between 250 and 300 °C, related to desorption of CO_2 from medium-strength basic sites. (iii) A broad desorption peak at 450 °C that it attributed to CO_2 desorption from sites with strong basicity. A deconvolution procedure was applied to quantify the basic density corresponding to the different sites. The results of this analysis are summarized in Table 3. By analyzing the samples with the third metal embedded, those with Li showed the highest basic

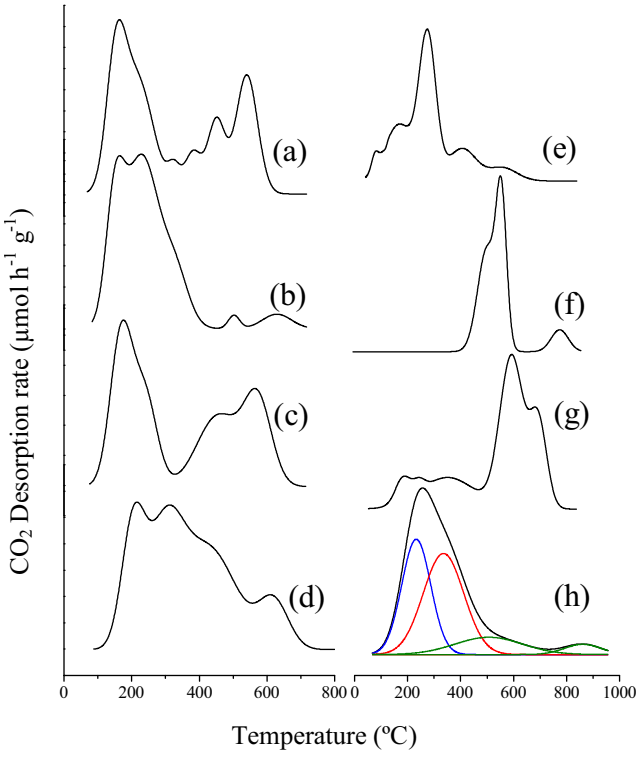

Fig. 5. CO_2 desorption profiles at programmed temperature of the OMM: (a) $(Mg\text{-}Al)_C$, (b) $(Li\text{-}Mg\text{-}Al)_C$, (c) $(K\text{-}Mg\text{-}Al)_C$, (d) $(Cs\text{-}Mg\text{-}Al)_C$, (e) $(Mg\text{-}Al)_I$, (f) $(Li\text{-}Mg\text{-}Al)_I$, (g) $(K\text{-}Mg\text{-}Al)_I$ y (h) $(Cs\text{-}Mg\text{-}Al)_I$.

site density. The mixed metal oxide with Li incorporated by the co-precipitation method presented the highest medium-strength basic site density. Meanwhile, oxides with K and Cs showed strong and weak sites similar to Mg-Al oxide, but both presented density values of medium-strength basic sites significantly lower. This could be due to the lower amount of third metal incorporated in these oxides.

Table 3
Basicity of OMM expressed as basic site density (strength: weak, medium and strong).

Sample	Basic sites density ($\mu mol\ CO_2\ g^{-1}$)			
	OH^-	O^{2-}		Total
	Weak	Medium	Strong	
$(Mg\text{-}Al)_C$	3.5	5.5	7.0	16,0
$(Li\text{-}Mg\text{-}Al)_C$	3.0	9.0	3.0	15,0
$(K\text{-}Mg\text{-}Al)_C$	3.5	2.0	5.5	11.0
$(Cs\text{-}Mg\text{-}Al)_C$	3.0	4.0	7.0	14.0
$(Mg\text{-}Al)_I$	0,0	0.5	0.0	0.5
$(Li\text{-}Mg\text{-}Al)_I$	0.0	0.0	18.0	18.0
$(K\text{-}Mg\text{-}Al)_I$	1.0	3.5	9.5	14.0
$(Cs\text{-}Mg\text{-}Al)_I$	1.0	1.0	0.5	2.5

To confirm the chemical nature of the surface basic sites in the samples, FT-IR spectra of CO_2 adsorbed at room temperature were taken after sequential evacuation at increasing temperature. The spectra were recorded after evacuation of CO2 at different temperatures: 25, 100, 200, 300 and 400 °C. By this technique, it was possible to identify three adsorbed CO_2 species: bicarbonate (Bic) formed on the OH^- groups (weak basic sites), bidentate carbonate (BC) for medium-strength basic sites and unidentate carbonates (UC) corresponding to strong basic sites interacting, in both cases, with O^{2-} and the corresponding metal.

In Fig. 6 the spectra of the MMO Mg-Al and Al-Mg-Li obtained by co-precipitation are shown. These materials have the highest medium basic site density. Bicarbonate bands correspond to C—OH species at 1220 cm^{-1}, and symmetric and asymmetric O—C—O mode at 1480 cm^{-1} and 1650 cm^{-1}, respectively. These species disappear after evacuation at 200 °C, evidencing their weak basic character. On the other hand, the bidentate carbonate bands at 1320–1340 cm^{-1} and 1610–1630 cm^{-1} are present, whereas the unidentate carbonate is observed from 1360 to 1400 cm^{-1} and at 1510–1560 cm^{-1}, in both cases requiring O^{2-} ions on the surface [41–44].

These species disappear after evacuation at 400 °C, evidencing their medium and strong basic character. Thus, the regions corresponding to the weak basic sites are attenuated more easily than those corresponding to the sites of high basic strength.

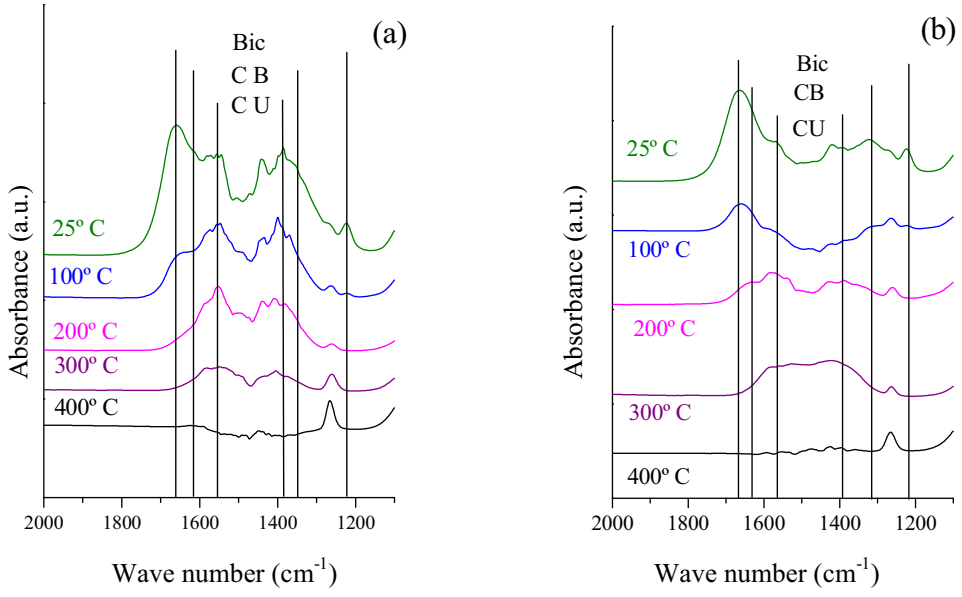

Fig. 6. FT-IR spectra of CO_2 adsorbed after evacuation at 25, 100, 200, 300 and 400 °C on (a) $(Mg\text{-}Al)_C$, (b) $(Li\text{-}Mg\text{-}Al)_C$.

Table 4
Catalytic activity results from glycerol transesterification with methyl stearate.

Catalyst	Stearate conversion (mol%)	Selectivity (mol%)			Yield
		MG	DG	TG	MG
$(Mg\text{-}Al)_C$	79	87	13	0	69
$(Li\text{-}Mg\text{-}Al)_C$	94	83	16	1	78
$(Li\text{-}Mg\text{-}Al)_I$	87	66	34	0	57
$(K\text{-}Mg\text{-}Al)_C$	90	83	16	1	74
$(K\text{-}Mg\text{-}Al)_I$	76	63	37	0	48
$(Cs\text{-}Mg\text{-}Al)_C$	91	80	18	2	73

3.1.6. Catalytic activity

All samples were tested in the methyl stearate (ME) glycerolysis reaction at 220 °C, using a reactant mixture of Gly/ME = 6.0/1.0 (molar ratio) and a catalyst/reactant weight percentage (W_{cat}/W_{Gly+ME}) of 4%. After the reactant mixture emulsification and the reaction temperature were reached, the catalyst was added. Indeed, previous studies showed that the reaction time required to reach greatest conversions was 6 h.

Table 4 shows the results of catalytic activity (conversion, selectivity and yield) of the MMO obtained by both methods. The results listed in this table are those that showed conversion greater than 75%. As can be seen, the MMO obtained by both methods showed low or null glyceryl tristearate (TG) production percentage.

All catalysts showed high conversions and selectivities to glyceryl monostearate. The oxides obtained by the impregnation method exhibited lower conversion and selectivity than those obtained by co-precipitation. MMO with Li incorporated by co-precipitation gave the highest yield to glyceryl monostearate. The main effect of Li loading was the improvement of the catalyst activity for the glycerolysis reaction. This fact correlates with the highest density of medium basic sites. Therefore, it may be concluded that the monoglyceride synthesis on the oxide $(LiMgAl)_C$ is mainly promoted by the maximum density of medium strength basic sites.

Therefore, the incorporation of an alkaline metal such as Lithium, in a specific load, is a way to improve the performance of the material resulting in an advantage about other authors reported [45,46].

4. Conclusions

It was possible to synthesize hydrotalcite-like compounds modified with monovalent metal ions (Li, K or Cs)/by the co-precipitation method. Meanwhile, by the wet impregnation method, it was not possible to completely reconstruct the LDH structure, showing a partial recovery of the layer structure.

The MMO obtained by heat treatment presented MgO periclase phase as well as alkali metal oxides.

In all samples, MMO specific surface areas were greater than those of LDH due to the dehydroxylation of brucite-type layers together with the elimination of carbonate ions from the interlayer space.

The percentage of metal incorporation was higher for materials modified with Li than for those modified with K and Cs. This fact can be attributed to the lower size of ionic radii.

All oxides presented basic properties. Those obtained by the co-precipitation method revealed a basic site density greater than those obtained by the impregnation method, except the sample with K incorporated $(K\text{-}Mg\text{-}Al)_I$.

The sample with Li incorporated by the co-precipitation method $(Li\text{-}Mg\text{-}Al)_C$ showed the greatest medium basic site density, which was reflected in an increased yield to monoglycerides. Consequently, it could be argued that the medium basic sites are responsible for the catalytic activity observed.

Acknowledgements

The authors are grateful to Universidad Tecnológica Nacional for the financial support. Thanks are also given to ANPCyT for the purchase of the SPECS multitechnique analysis instrument (PME8-2003) and to J. D. Fernández for assistance with surface area measurements.

References

[1] J.N. Chheda, G.W. Huber, J.A. Dumesic, Angew. Chem. Int. 46 (2007) 7164–7183.
[2] J.C. Juan, D.A. Kartika, T.Y. Wu, T.-Y.Y. Hin, Bioresour. Technol. 102 (2011) 452–460.
[3] M.J. Climent, A. Corma, P. De Frutos, S. Iborra, M. Noy, A. Velty, J. Catal. 269 (2010) 140–149.
[4] W. Hu, D. Knight, B. Lowry, A. Varma, Ind. Eng. Chem. Res. 49 (2010) 10876–10882.
[5] A. Tsuji, K.T.V. Rao, S. Nishimura, A. Takagaki, K. Ebitani, ChemSusChem 4 (2011) 542–548.
[6] S. Zhu, Y. Zhu, S. Hao, L. Chen, B. Zhang, Y. Li, Catal. Lett. 142 (2012) 267–274.
[7] S. Xia, Z. Yuan, L. Wang, P. Chen, Z. Hou, Bioresour. Technol. 104 (2012) 814–817.
[8] Z. Yuan, J. Wang, L. Wang, W. Xie, P. Chen, Z. Hou, X. Zheng, Technology 101 (2010) 7088–7092.
[9] E. Tsukuda, S. Sato, R. Takahashi, T. Sodesawa, Catal. Commun. 8 (2007) 1349–1353.
[10] M. Ayoub, M.S. Khayoon, A.Z. Abdullah, Bioresour. Technol. 112 (2012) 308–312.
[11] P. Felizardo, J. Machado, D. Vergueiro, M.J.N. Correia, J. Pereira Gomes, J. Moura Bordado, Fuel Process. Technol. 92 (2011) 1225–1229.
[12] D. Stošić, S. Bennici, S. Sirotin, C. Calais, J.-L. Couturier, J.-L. Dubois, A. Travert, A. Auroux, Appl. Catal. A: Gen. 447–448 (2012) 124–134.
[13] C. García-Sancho, R. Moreno-Tost, J.M. Mérida-Robles, J. Santamaría-González, A. Jiménez-López, P. Maireles-Torres, Catal. Today 167 (2011) 84–90.
[14] P. Guerrero-Urbaneja, C. García-Sancho, R. Moreno-Tost, J. Mérida-Robles, J. Santamaría-González, A. Jiménez-López, P. Maireles-Torres, Appl. Catal. A: Gen. 470 (2014) 199–207.
[15] N. Pasupulety, G.L. Rempel, F.T.T. Ng, Appl. Catal. A: Gen. 489 (2015) 77–85.
[16] Q. Liu, C. Wang, W. Qu, B. Wang, Z. Tiana, H. Ma, R. Xu, Catal. Today 234 (2014) 161–166.
[17] E. Borodina, S.I. Karpov, V.F. Selemenev, W. Schwieger, S. Maracke, M. Fröba, F. Rößner, Microporous Mesoporous Mater. 203 (2015) 224–231.
[18] G. Centi, S. Perathoner, Microporous Mesoporous Mater. 107 (2008) 3–15.
[19] X. Lin, R. Li, M. Lu, C. Chen, D. Li, Y. Zhan, L. Jiang, Fuel 162 (2015) 271–280.
[20] K. Morimoto, K. Tamura, S. Anraku, T. Sato, M. Suzuki, H. Yamada, J. Solid State Chem. 228 (2015) 221–225.
[21] J.L. Shumaker, C. Crofcheck, S.A. Tackett, E. Santillan-Jimenez, T. Morgan, Y. Ji, M. Crocker, T.J. Toops, Appl. Catal. B: Environ. 82 (2008) 120–130.
[22] M.G. Álvarez, A.M. Segarra, S. Contreras, J.E. Sueiras, F. Medina, F. Figueras, Chem. Eng. J. 161 (3) (2010) 340–345.
[23] M. Crivello, C. Pérez, J. Fernández, G. Eimer, E. Herrero, S. Casuscelli, E. Rodríguez-Castellón, Appl. Catal. A: Gen. 317 (2007) 11–19.
[24] N. Bálsamo, S. Mendieta, M. Oliva, G. Eimer, M. Crivello, Procedia Mater. Sci. 1 (2012) 506–513.
[25] M.J. Climent, A. Corma, P. De Frutos, S. Iborra, M. Noy, A. Velty, P. Concepción, J. Catal. 269 (2010) 140–149.
[26] D.G. Cantrell, L.J. Gillie, A.F. Lee, K. Wilson, Appl. Catal. A: Gen. 287 (2005) 183–190.
[27] P.G. Belelli, C.A. Ferretti, C.R. Apesteguía, R.M. Ferullo, J.I. Di Cosimo, J. Catal. 323 (2015) 132–144.
[28] C. Ferretti, A. Soldano, C. Aspeteguía, J. Di Cosimo, Chem. Eng. J. 161 (2010) 346–354.
[29] A. Corma, S. Iborra, S. Miquel, J. Primo, J. Catal. 173 (1998) 315–321.
[30] C.A. Ferretti, C.R. Apesteguía, J.I. Di Cosimo, J. Argentine Chem. Soc. 98 (2011) 16–28.
[31] A. Mantilla, F. Tzompantzi, J.L. Fernández, J.A.I. Díaz Góngora, R. Gómez, Catal. Today 150 (2010) 353–357.
[32] M. Domine, M. Hernández-Soto, Y. Pérez, Catal. Today 159 (2011) 2–11.
[33] O.D. Pavel, R. Zăvoianu, R. Bîrjega, E. Angelescu, Mater. Res. Bull. 45 (2010) 1106–1111.
[34] T. Stanimirova, G. Kirov, Appl. Clay Sci. 22 (2003) 295–301.
[35] K.H. Goh, T.-t. Lim, Z. Dong, Water Res. 42 (2008) 1343–1368.
[36] Q. Guo, E. Reardon, Appl. Clay Sci. 56 (2012) 7–15.
[37] B.R. Venugopal, C. Shivakumara, M. Rajamathi, Solid State Sci. 9 (2007) 287–294.
[38] M. Mokhart, A. Inayat, J. Ofili, W. Schieger, Appl. Clay Sci. 50 (2010) 176–181.
[39] F. Cavani, F. Trifiro, Appl. Catal. A 133 (1995) 219–239.
[40] E.L.G. Oliveira, C.A. Grande, A.E. Rodrigues, Sep. Purif. Technol. 62 (2008) 137–147.
[41] M. León, E. Díaz, S. Bennici, A. Vega, S. Ordóñez, A. Auroux, Ind. Eng. Chem. Res. 49 (2010) 3663–3671.

[42] P. Kuśtrowski, D. Sułkowska, L. Chmielarz, A. Rafalska-Łasocha, B. Dudek, R. Dziembaj, Microporous Mesoporous Mater. 78 (2005) 11–22.
[43] J.I. Di Cosimo, V.K. Díez, M. Xu, E. Iglesia, C.R. Apesteguía, J. Catal. 178 (1998) 499–510.
[44] R. Philipp, K. Fujimoto, J. Phys. Chem. 96 (1992) 9035–9039.
[45] A. Corma, Sh B.A. Hamid, S. Iborra, A. Velty, J. Catal. 234 (2005) 340–347.
[46] C.A. Ferretti, C.R. Apesteguía, J.I. Di Cosimo, Appl. Catal. A: Gen. 399 (2011) 146–153.